ELSEVIER

Contents lists available at ScienceDirect

# **Additive Manufacturing**

journal homepage: www.elsevier.com/locate/addma



## Research Paper

# Online droplet anomaly detection from streaming videos in inkjet printing



Luis Javier Segura, Tianjiao Wang, Chi Zhou\*, Hongyue Sun\*

Department of Industrial and Systems Engineering, University at Buffalo, SUNY Buffalo, NY 14260, United States

ARTICLE INFO

Keywords:
Bayesian online change detection
Online tensor factorization
Inkjet printing
Streaming data

#### ABSTRACT

Inkjet printing (IJP) has demonstrated its capabilities to produce high-quality and high-resolution parts, such as sensors, bio-chips, etc., with outstanding functionality. However, the quality of the printed parts can be endangered by the abnormal droplet jetting behaviors, which are substantially governed by the process dynamics and ambient conditions. Additionally, the droplet behaviors extensively define the final drop deposition quality in IJP. Timely capturing and identifying abrupt anomalies that the ejected droplets may suffer from are primordial for the quality assurance of the printed parts. Machine vision systems are able to record the droplet videos during IJP. Nevertheless, it is challenging to timely detect the anomalies from the collected droplet videos. The objective of this work is to build an analytical framework that allows for online droplet anomaly detection from droplet videos. There are several challenges that have not been addressed before: (1) the features of the droplet videos need to be extracted in an online fashion; and (2) there is no well-defined baseline to support the droplet anomalies detection, due to the complex process dynamics. Here, we propose a novel online framework to efficiently detect the anomalies from process streaming videos. In particular, we extend the multivariate Bayesian online change detection (BOCD) framework to high-dimensional data (i.e., tensor data of droplet videos) by leveraging online tensor factorization (OTF). OTF decomposes the streaming data into non-temporal and temporal low-dimensional factorization matrices. The non-temporal factorization matrices are deployed to extract the frame-specific temporal factorization matrix within a user-defined sliding window. Subsequently, the temporal factorization matrix for each frame is monitored with BOCD, which accurately detects anomalies in the streaming data. The proposed framework is demonstrated by detecting droplet anomalies from streaming data in IJP, showing excellent accuracy and efficiency.

## 1. Introduction

Additive manufacturing (AM) is a novel technology that will transform the way products are created and consumed [1]. Inkjet printing (IJP) is an AM process that is capable of producing parts with high-quality and high-resolution at micro-scale levels. Particularly, IJP is realized by the direct deposition of liquid-phase materials (e.g., ink/solution droplets at different concentrations) onto a substrate to form a finished part, as shown in Fig. 1 (a). Due to its noticeable characteristics (e.g., non-contact, high-resolution, low-cost, and scalability to large manufacturing area [2]), IJP has been able to produce functional parts, such as sensors, optic/electronic devices, biochips, and scaffolds [3], that have a wide range of applications in the electronics, energy, environment, and health areas. Among different IJP processes, the drop-on-demand (DOD) approach can deliver the highest resolution reported so far [4]. A suitable technology to supply droplets in DOD mode is the piezoelectric inkjet (PIJ) printing process (see Fig. 1), in

which the droplet behaviors (i.e., ejection, formation, and stability) play a crucial role towards the quality and repeatability of the printed parts. The dynamic droplet behaviors are governed by the driving electrical signal, process back-pressure, ink/solution properties (e.g., surface tension, viscosity, etc.), and the interaction among ink/solution, air, and substrate (e.g., wettability of the nozzle) [5]. For instance, different regimes of back-pressure directly affect the droplet sizes and velocities [6]. Additionally, external factors, such as air flow, vibration, ambient temperature, and humidity, can also induce severe droplet changes. Thus, it is paramount to have a system that is able to timely detect sudden droplet changes (e.g., droplet size, clogs, etc.) that may derive into product defects, such as dimension and shape off specifications (see Fig. 1(b)).

To preserve the quality of the IJP process, several statistical approaches, such as analysis of variance (ANOVA) and response surface methodology (RSM) have been used [7]. However, these studies have restricted their analysis in offline fashion, and online analysis still

E-mail addresses: chizhou@buffalo.edu (C. Zhou), hongyues@buffalo.edu (H. Sun).

<sup>\*</sup> Corresponding authors.

remains a critical challenge. The online droplet behavior can be recorded by computer vision systems, such as charged-couple device (CCD) camera and high-speed camera. For instance, Lies et al. [8] developed a vision assisted micro-filament detection method to monitor IJP. This analysis was limited to detecting whether a micro-filament is present or not. In addition, Wang et al. [9] developed a catadioptric stereo system to record droplet location but did not detect its shape changes. Actually, videos are represented by complex data structure, high-dimensionality and correlation characteristics, and are non-trivial to analyze [10]. For example, an image-based process monitoring using low-rank tensor decomposition was developed to monitor the steel tube manufacturing [10]. This and other monitoring approaches [11] need a set of baseline data (i.e., video of the process under control) to build the control charts offline, which cannot be used in the dynamic IJP processes since it is extremely hard to obtain the baseline data in IJP.

The objective of this paper is to build a framework that allows for online droplet anomaly detection from streaming tensor data (i.e., droplet videos). In particular, a CCD camera coupled with a magnifying lens was used to record the videos. Based on these videos, we achieve the online anomaly detection via extending the Bayesian online change detection (BOCD) [12] framework to tensor data. Specifically, tensors, multi-way generalizations of matrices, can multi-dimensional complex structure such as frames in a video recording. Here, the tensor dimensions increase considerably over time, and extracting features from dynamic tensors is challenging [13]. The merits of the proposed framework are three-fold: (a) we leverage the online Candecomp/Parafac (CP) tensor factorization (OnlineCP) [13] to analyze the IJP videos in real-time, which does not require baseline data to extract the features of videos. Hence, once the process is initialized, recurrent batch updates are not required even if the process baseline changes. (b) The OnlineCP incrementally tracks the CP decomposition of dynamic tensors, namely IJP video frames, while keeping a relatively constant computational time to process new incoming frames, and (c) the BOCD detects the IJP process anomalies in real-time without needing to know the baseline data.

As will be demonstrated in the Case Study section, the proposed framework is able to accurately detect the droplet anomalies in the incoming streaming data. Even though there are several methods dedicated to modeling high-dimensional data and monitoring the extracted features [10,14], to the best of our knowledge, this is the first study dedicated to the online detection of sudden changes from videos in IJP. The accuracy of the proposed framework is evaluated by comparing the actual versus detected anomalies in the recorded droplet videos under various conditions. The results showed that the proposed framework has high accuracy and efficiency. Such a framework is applicable to other processes, e.g., electrospinning and electrohydrodynamics IJP.

The organization of the paper is as follows. Section 2 will briefly review related studies on AM monitoring approaches. The proposed

framework will be described in Section 3. Section 4 will show the experimental results. Finally, Section 5 will conclude the paper and discuss the future work.

#### 2. Literature review

#### 2.1. Process improvements in IJP

IJP process has shown capabilities to produce parts with high accuracy at macro-scale and micro-scale levels. However, the printed parts' quality extensively relies on the stability and repeatability of the ejected droplets, which is not always the case and is intricate to achieve. Thus, several empirical and analytical studies have been realized in order to ensure IJP process performance [15–17].

Empirical models have been most widely explored. On one hand, several studies have been dedicated to tailoring ink/solutions to assure product consistency. For example, a high-throughput characterization methodology of fluid properties to predict droplet ejection for threedimensional IJP process was presented in [16]. Wang et al. [18] optimized the IJP process via surface engineering of the substrate, and printing parameters selection. Lee et al. [19] studied the suppression of clogging in IJP by optimizing the experimental ink/solution parameters (e.g., surface tension, viscosity). The Ohnesorge number was deployed to determine the jettability and non-jettability regimes in the printing of Zinc Oxide (ZnO). Similar studies can be seen in [20,21]. On the other hand, solution and process parameters have also been studied by empirical statistical methods, such as ANOVA and RSM [7], to improve the IJP process. Abu-Khalaf et al. [15] presented an approach for the optimization of geometry parameters of inkjet printed silver nano-particle traces on polydimethylsiloxane (PDMS) substrates using RSM. Rahul et al. [22] established a Taguchi and ANOVA optimization approach to improve the fabrication of thick ceramic coatings in the IJP process. Mueller et al. [23] studied the optimal parameters to improve the mechanical properties in 3D IJP process. A full factorial design was used and the improvements in mechanical properties (e.g., elastic modulus, ultimate tensile strength, etc.) were significant. Other similar studies can be seen in [24,25].

Analytical models have also been used to predict and control the droplet dynamics and quality of the printed parts in the IJP process. For instance, Morrison et al. [26] investigated the effects of viscoelasticity on drop generation in IJP since ink/solution's concentration and molecular weight must be carefully chosen for optimal printing. Van der Bos et al. [27] realized a comparison of a numerical simulation based on the slender jet approximation of the Navier-Stokes equations and an experimental approach, which showed accurate agreement and was beneficial for the printing process. More examples can be seen in [28, 29].

Although the aforementioned methods have shown to be beneficial

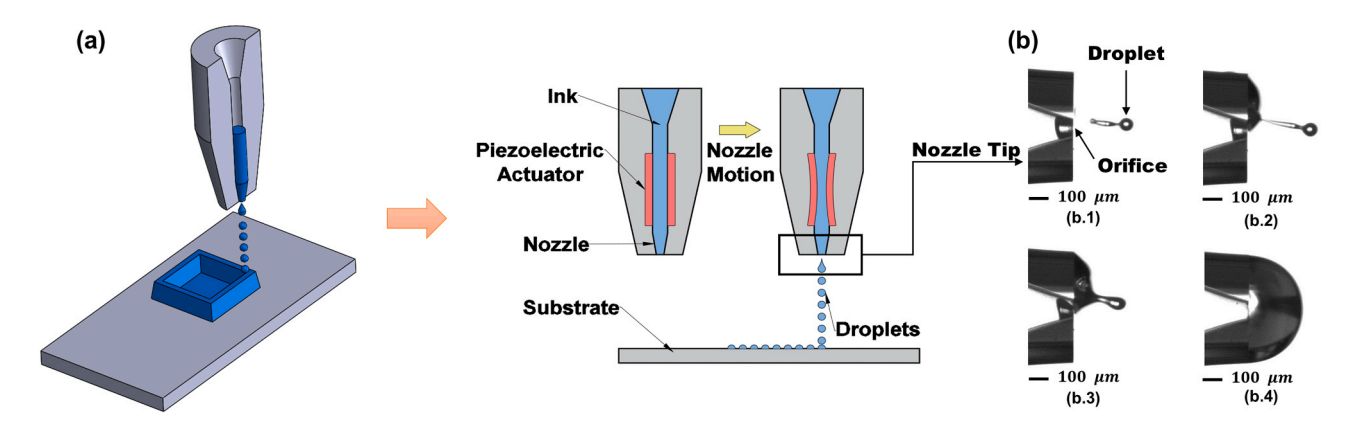


Fig. 1. A Scheme of the inkjet printing process (IJP): (a) Piezoelectric inkjet (PIJ) printing process, and (b) Representative PIJ droplet anomalies: (b.1) Normal, (b.2), Off-trajectory, (b.3) Attached to the nozzle, and (b.4) Blockage.

to improving the IJP process, they are performed offline, therefore preventing them from their applicability in real-time monitoring and control.

#### 2.2. Process monitoring approaches

Image sensors, such as borescope, CCD cameras, etc., are able to provide a great amount of process information. However, this information has not been adequately exploited. In particular, image sensor information is usually of high frequency and high dimension, and processing this information is challenging. To address this, dimensional reduction techniques, such as principal component analysis (PCA) and unfolded PCA, are utilized to extract features that will be used for later analysis. For instance, Khanzadeh et al. [30] presented a process monitoring of metal-based AM using a multilinear PCA (MPCA) feature extraction approach, which was applied to thermal image streams. See other related works in [31–33]. However, these techniques break the original structure of the data, and this might affect the anomalies detection accuracy.

Alternatively, tensor decomposition methods preserve the structure of the original data and have been recently explored in image-based process monitoring [10,14,33]. Most proposed methods used alternating least squares (ALS) to solve the formulation of the tensor decomposition, which can be time consuming if continuous updates are needed due to complex process dynamics, as in the case of IJP. In addition, the available frameworks require a baseline to determine the monitoring statistics and control limits for subsequent anomalies detection, which is a complex task to achieve. To avoid the baseline data requirement, online feature extraction is paramount. Hawkins et al. [34] developed a streaming tensor factorization approach via variational Bayesian inference, which enjoys high accuracy but lacks computational efficiency. See other methods in [35,36]. Conversely, a faster approach, namely OnlineCP, is shown by Zhou et al. [13] and will be deployed here. In particular, this approach is capable to incrementally track the CP decompositions of dynamic tensors, e.g., IJP droplet video, with an

arbitrary number of dimensions and has shown good stability, efficiency, and scalability.

Once the online features are available, change point (i.e., anomaly) detection methods are able to detect anomalies without needing the baseline data [37,38]. To achieve the online change detection, Adams et al. [39] developed a BOCD method, where priors for the segment's parameters and for the length of the segment are needed for the Bayesian inference. Kawahara et al. [40] presented an online method for change point detection in sequential data by deploying direct density-ratio estimation. Other examples can be seen in [41,42]. Nonetheless, most of these methods can only be applied to univariate sequential data and are not feasible to leverage the features extracted from online tensor factorization. Thus, multivariate change point detection methods are imperative to identify abrupt anomalies in streaming data. The BOCD presented in [39] has shown sufficient robustness and has been expanded to detecting abrupt anomalies in multivariate streaming data [12]. We will integrate the BOCD and OnlineCP in this paper to efficiently and accurately detect abrupt anomalies from droplet videos in the IJP process.

#### 3. Proposed framework

## 3.1. Overview of the proposed framework

A schematic illustration of the proposed framework is presented in Fig. 2. Fig. 2 (a) shows the IJP setup. The variations of ink/solution, process, and ambient parameters may induce droplet anomalies (see examples in Fig. 2 (b)), hence affecting the quality of the printed parts. As illustrated in Fig. 2 (c), we record droplet videos with a CCD camera to capture the droplet behaviors. The high-dimensional videos are used as input data to detecting anomalies. In particular, the videos are firstly pre-processed as shown in Fig. 2 (d.1) for later analysis. After that, online tensor factorization (OTF), namely OnlineCP [13], is deployed for feature extraction (see Fig. 2 (d.2)) in a sliding window (sw). The OnlineCP can efficiently process streaming data (e.g., new video

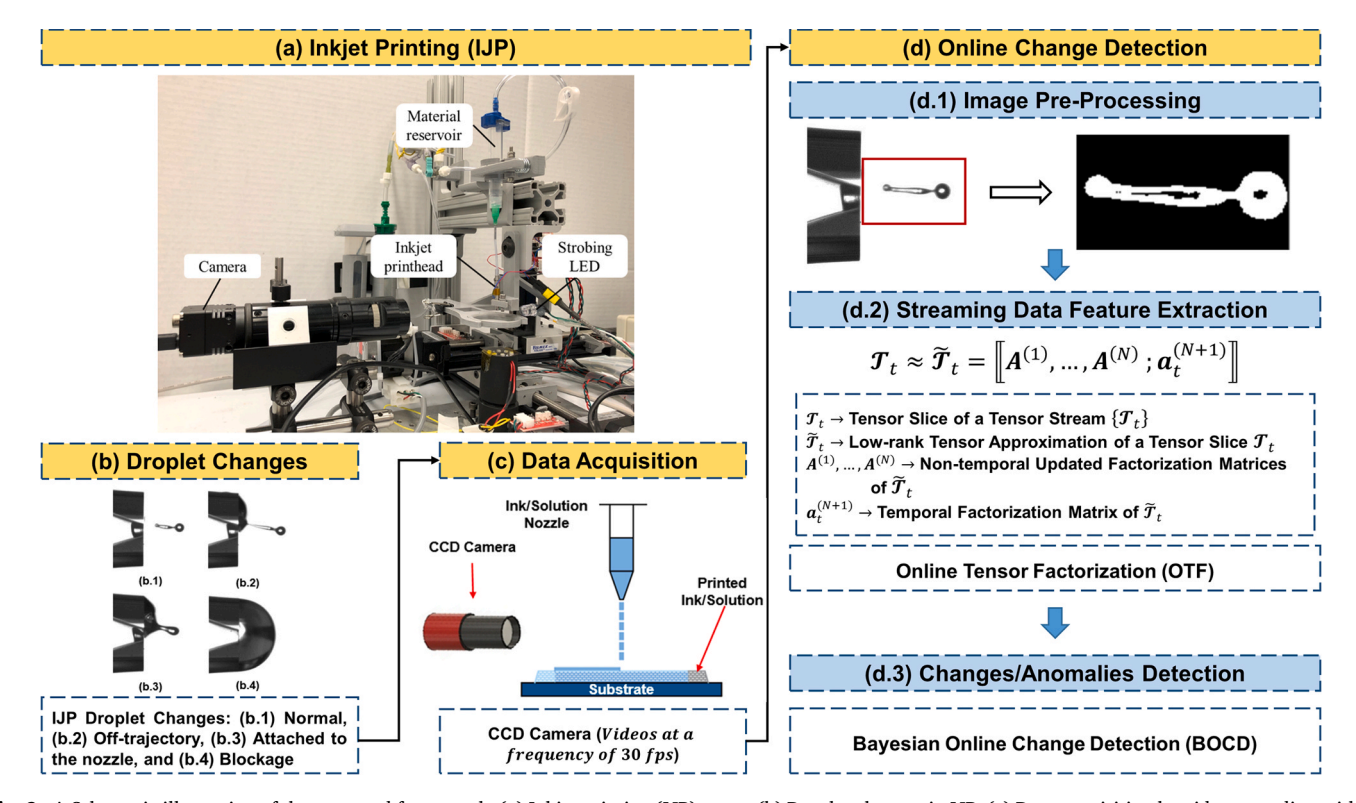


Fig. 2. A Schematic illustration of the proposed framework: (a) Inkjet printing (IJP) setup, (b) Droplet changes in IJP, (c) Data acquisition by video recording with a CCD camera, and (d) Online change detection via OTF and BOCD.

frames). After OnlineCP, we extract the non-temporal factorization matrices, specifically  $\mathbf{A}^{(1)}, ..., \mathbf{A}^{(N)}$  in Fig. 2 (d.2), and use them to update the temporal factorization matrix, namely  $\mathbf{a}^{(N+1)}$ , in the specified sw. We then use BOCD to detect anomalies in each frame based on the updated temporal factorization matrix. The aforementioned OnlineCP and BOCD are recursively performed until the end of the streaming data, as shown in Algorithm 1.

In the proposed method, image pre-processing, streaming data feature extraction, and anomalies detection are performed online. Thus, real-time process control could be feasible, which is out of the scope of this paper and will be investigated in the future. The following section is dedicated to explaining the details of the proposed framework.

## 3.2. Setup for video data acquisition

The hardware of our video collection system is shown in Fig. 2 (a). The droplets are generated by a piezo-based micro-dispensing nozzle (MicroFab Inc.). This print-head system is suitable for typical Newtonian ink/solutions, such as water and glycerol. The nozzle's diameters are 50  $\mu m$  and 100  $\mu m$ , as presented in Table 1. The droplet videos are captured by a CCD camera (Sensor Technologies Inc.) coupled with a magnification lens. The video resolution is  $480 \times 640$  pixels. Finally, strobing technology is utilized to capture the droplet at a specific instance after the droplet is ejected, as shown in Fig. 2 (d.1). The strobe delay time, time between the jetting signal and lighting signal of the LED for illumination, was set as shown in Table 1.

#### 3.3. OnlineCP decomposition

The online droplet behaviors are crucial for IJP, and it is challenging to extract the behavior information from real-time videos. OTF is a powerful tool to address this issue by exploring and extracting the underlying structure of the multi-way data [13]. The objective of OTF is to approximate high-dimensional tensors with the tensor product of low-dimensional non-temporal factorization matrices (e.g.,  $\mathbf{A}^{(1)}$ , ...,  $\mathbf{A}^{(N)}$ ) and temporal factorization matrix (e.g.,  $\mathbf{a}_t^{(N+1)}$ ) in an online manner, as shown in Fig. 2 (d.2). OTF has been studied under several low-rank tensor models, such as Tucker [43] and CP [13] decomposition. We apply the CP decomposition in this study due to its sparse core tensor structure.

Let  $\{\mathcal{T}_t\}$  be a temporal sequence (i.e., droplet video frames in our case) of N-way tensors, where  $t \in \mathbb{N}$  is the time index and  $\mathcal{T}_t$  of dimension  $I_1 \times I_2 \times \ldots \times I_N$  is a slice (i.e., frame) of the multi-way stream, see Fig. 3 for an illustration of the data structure. Specifically, a new incoming slice  $\mathcal{T}_{t_{new}}$  can be approximated by the CP decomposition:  $\widetilde{\mathcal{T}}_{t_{new}} = [A^{(1)}, \ldots, A^{(N)}; a_{t_{new}}^{(N+1)}]$ , where  $[[\bullet]]$  is the tensor product,  $A^{(N)} \in \mathbb{R}^{I_N \times R}$  are the non-temporal factorization matrices,  $a_{t_{new}}^{(N+1)} \in \mathbb{R}^{t_{new} \times R}$  denotes the frame-specific temporal factorization matrix (e.g.,  $t_{new} = 1$  for a new single incoming video frame), and R is the tensor rank. The CP decomposition problem can be solved via ALS. However, the computation time of ALS is intractable for high-dimensional streaming data. We use the OnlineCP decomposition [13] to tackle this problem. Without loss of generality, the onlineCP is illustrated with a third-order online tensor  $\{\mathcal{T}_t\} \in \mathbb{R}^{I \times J \times (t_{old} + t_{new})}$ , where  $t = t_{old} + t_{new}$ , as shown in Fig. 4.  $\{\mathcal{T}_t\}$  is expanded from  $\{\mathcal{T}_{t_{old}}\} \in \mathbb{R}^{I \times J \times t_{old}}$  by appending new

 Table 1

 Experimental Settings for the IJP Video Collection.

Video	Nozzle (μm)	Back-pressure (in H <sub>2</sub> O)	Length (seconds)	Delay (μs)
(1)	100	[-6,3]	121	200
(2)	50	[-3.5, 0]	40	250
(3)	100	[-10, 2]	40	250
(4)	100	4	100	250

incoming data  $\{\mathcal{T}_{t_{new}}\}\in\mathbb{R}^{I imes J imes t_{new}}$ , which can be a tensor or a set of multiple tensors. It is assumed that  $t_{new}\ll t_{old}$ . The CP decomposition of  $\{\mathcal{T}_{t_{old}}\}$  is approximately  $\{\widetilde{\mathcal{T}}_{t_{old}}\}=[A_{t_{old}}^{(1)},A_{t_{old}}^{(2)},A_{t_{old}}^{(3)}]$ , and the ultimate objective is to find the CP decomposition  $[[A^{(1)},A^{(2)},A^{(3)}]]$  of  $\{\mathcal{T}_t\}$ .

The temporal factorization matrix  $A^{(3)}$  can be computed by:

$$A^{(3)} \leftarrow \arg \min_{A^{(3)}} \frac{1}{2} \| \{ \mathcal{T}_t \}_{(3)} - A^{(3)} (A^{(2)} \odot A^{(1)})^T \|_F^2$$

$$= \arg\min_{\mathbf{A}^{(3)}} \frac{1}{2} \left\| \begin{bmatrix} \{\mathcal{T}_{t_{old}}\}_{(3)} - \mathbf{A}_{t_{old}}^{(3)} (\mathbf{A}^{(2)} \odot \mathbf{A}^{(1)})^T \\ \{\mathcal{T}_{t_{new}}\}_{(3)} - \mathbf{A}_{t_{new}}^{(3)} (\mathbf{A}^{(2)} \odot \mathbf{A}^{(1)})^T \end{bmatrix} \right\|_{E}^{2}, \tag{1}$$

where  $\| \bullet \|_F$  is the Frobenius norm,  $\odot$  is the Khatri-Rao product.  $\boldsymbol{A}^{(1)}$  and  $\boldsymbol{A}^{(2)}$  are fixed as  $A_{t_{old}}^{(1)}$  and  $A_{t_{old}}^{(2)}$  from the previous time. The first row in Eq. (1) is minimized by  $A_{t_{old}}^{(3)}$ , and the optimal solution to minimize the second row is  $A_{t_{new}}^{(3)} = \{\mathcal{T}_{t_{new}}\}_{(3)} \left(\left(A_{t_{old}}^{(2)} \odot A_{t_{old}}^{(1)}\right)^T\right)^\dagger$ , here  $\dagger$  represents the Moore-Penrose pseudoinverse, and finally  $A^{(3)}$  (see line 5 in Algorithm 1) is updated as:

$$\mathbf{A}^{(3)} = \begin{bmatrix} \mathbf{A}_{t_{old}}^{(3)} \\ \mathbf{A}_{t_{new}}^{(3)} \end{bmatrix}$$

$$= \begin{bmatrix} \mathbf{A}_{t_{old}}^{(3)} \\ \{\mathcal{T}_{t_{new}}\}_{(3)} \left( \left( \mathbf{A}_{t_{old}}^{(2)} \odot \mathbf{A}_{t_{old}}^{(1)} \right)^T \right)^{\dagger} \end{bmatrix}$$

$$(2)$$

Subsequently, the non-temporal factorization matrices  $A^{(1)}$  and  $A^{(2)}$  need to be updated. For instance,  $A^{(1)}$  is updated by fixing  $A^{(2)}$  and  $A^{(3)}$  (see line 3 in Algorithm 1):

$$\mathbf{A}^{(1)} \leftarrow \arg\min_{\mathbf{A}^{(1)}} \frac{1}{2} \| \{ \mathcal{T}_t \}_{(1)} - \mathbf{A}^{(1)} (\mathbf{A}^{(2)} \odot \mathbf{A}^{(3)})^T \|_F^2$$
 (3)

Define two auxiliary matrices  $P^{(1)} = P_{t_{old}}^{(1)} + P_{t_{new}}^{(1)}$  and  $Q^{(1)} = Q_{t_{old}}^{(1)} + Q_{t_{new}}^{(1)}$  in  $\mathbb{R}^{(N)}$ , where  $P_{t_{old}}^{(1)} = \{\mathcal{T}_{t_{old}}\}_{(1)} \left(A_{t_{old}}^{(3)} \odot A_{t_{old}}^{(2)}\right)$ ,  $P_{t_{new}}^{(1)} = \{\mathcal{T}_{t_{new}}\}_{(1)} \left(A_{t_{new}}^{(3)} \odot A_{t_{old}}^{(2)}\right)$ ,  $Q_{t_{old}}^{(1)} = \left(A_{t_{old}}^{(3)} A_{t_{old}}^{(3)}\right)^{\circ} \left(A_{t_{old}}^{(2)} A_{t_{old}}^{(2)}\right)$  and  $Q_{t_{new}}^{(1)} = \left(A_{t_{new}}^{(3)} A_{t_{new}}^{(3)}\right)^{\circ} \left(A_{t_{old}}^{(2)} A_{t_{old}}^{(2)}\right)$ , where  $\circ$  is the Hadamard product. The auxiliary matrices need to be initialized before the streaming data starts progressing. To this end, a small partition  $\{\mathcal{T}_{\tau}\} \in \mathbb{R}^{I \times J \times \tau}$  of data, containing few  $\tau$  slices/video frames  $\mathcal{T}$ , are utilized. Naturally,  $\tau \ll t_{old}$ . The process can be generalized for any number of dimensions [13].

Then, the update of  $A^{(1)}$  (see line 3 in Algorithm 1) is executed via [13].

$$A^{(1)} \leftarrow P^{(1)} Q^{(1)^{-1}} \tag{4}$$

Note that  $P_{t_{old}}^{(1)}$  and  $Q_{t_{old}}^{(1)}$  are computed from the past data, hence only  $P_{t_{new}}^{(1)}$  and  $Q_{t_{new}}^{(1)}$  need to be incrementally updated, thus considerably saving computational resources.  $A^{(2)}$  can be updated in similar a fashion to  $A^{(1)}$  [13], see line 4 in Algorithm 1.

After the OnlineCP is executed, the non-temporal factorization matrices, namely  $\mathbf{A}^{(1)}$  and  $\mathbf{A}^{(2)}$ , are updated and deployed to perform the detection feature extraction within the user-defined sw (see lines 2–8 in Algorithm 1). We ultimately obtain the temporal factorization matrix  $\mathbf{a}_{t-i+1}^{(N+1)} \in \mathbb{R}^{sw \times R}$ , where  $i \in [1, sw]$  (see line 7 in Algorithm 1), and the temporal sequence at each sw can be reconstructed as  $\{\mathcal{T}_{sw}\} = [\mathbf{A}^{(1)}, \mathbf{A}^{(2)}; \mathbf{a}_{t-i+1}^{(N+1)}]$ . In this way, we assure that the features are extracted from the same vector space. The monitoring statistics (see Fig. 5 (b.2)) are allocated in the temporal factorization matrix and are the inputs for subsequent analysis.

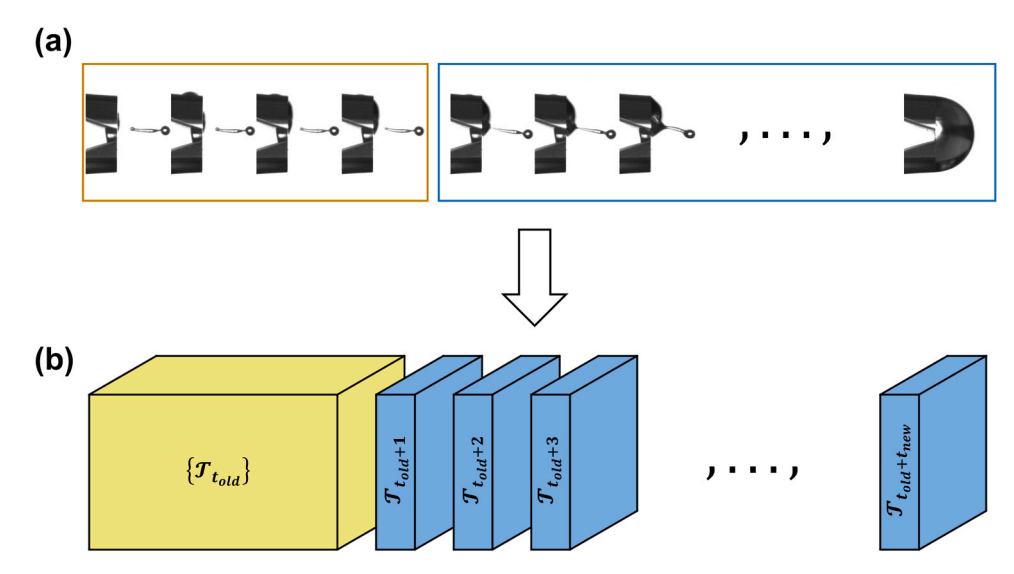


Fig. 3. Streaming data illustration (Third-order Tensor): (a) LJP frames sequence and (b) Sequence representation.

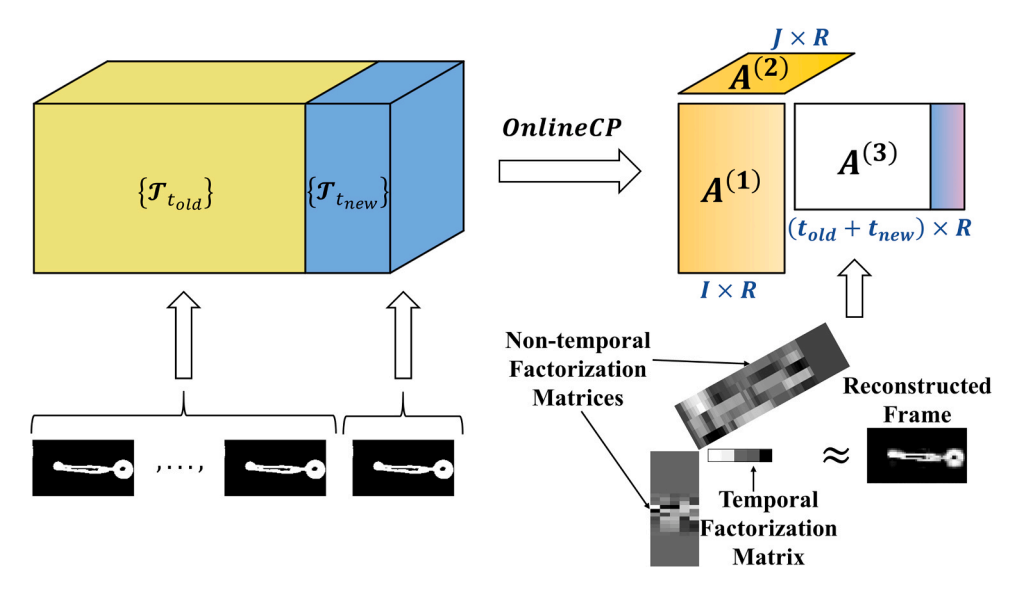


Fig. 4. OnlineCP tensor decomposition scheme.

## 3.4. Bayesian online change detection

## Algorithm 1. Online video anomaly detection.

```
input: Streaming data \{\mathcal{T}_t\}, rank R, sliding window sw, initialized auxiliary matrices P^{(N)}, Q^{(N)} output: Anomaly detected (AD)
1 repeat
2 Detection feature extraction;
3 Update A^{(1)} = P^{(1)}Q^{(1)^{-1}} by fixing A^{(2)} and A^{(3)};
4 Update A^{(2)} = P^{(2)}Q^{(2)^{-1}} by fixing A^{(1)} and A^{(3)};
5 Update A^{(3)} = \begin{bmatrix} A_{i,ad}^{(3)} \\ A_{inot}^{(3)} \end{bmatrix} by fixing A^{(1)} and A^{(2)}, via Eq. (2);
6 for i \leftarrow 1 to sw do
7 Update a_{t-i+1}^{(N+1)} = \{\mathcal{T}_t\}_{(3)} \left( \left( A^{(2)} \odot A^{(1)} \right)^T \right)^{\dagger};
8 end
9 Anomaly detection within each sw;
10 for t \leftarrow 1 to sw do
11 Compute predictive probability, p(a_t|\mu^{(r_t)}, \Sigma^{(r_t)});
12 Compute posterior probability, p(r_t|a_{1:t}, r_{t-1});
```

(continued on next column)

## (continued)

```
13 Current length, r_t = \max(p(r_t|a_{1:t}, r_{t-1}));
14 if r_t < r_{t-1} then
15 lastAD = t;
16 else
17 continue;
18 end
19 Update parameters \eta_t
20 end
21 until \mathcal{T}_{t_{new}} is finished;
22 return Detected\ ADs
```

Once the monitoring statistics are extracted, a mechanism to find the anomalies in the IJP videos is required. Although offline detection algorithms usually lead to more accurate results, online detection algorithms are necessary for dynamic systems that require instantaneous responses [38], as shown in Fig. 5.

BOCD assumes that the temporal factorization matrix can be modeled with a certain parametric function in each sliding window (see lines 9–20 in Algorithm 1), and abrupt anomalies in the droplet videos are detected when the model's parameters vary. In particular, based on the prior probability density functions for the segment's parameters and

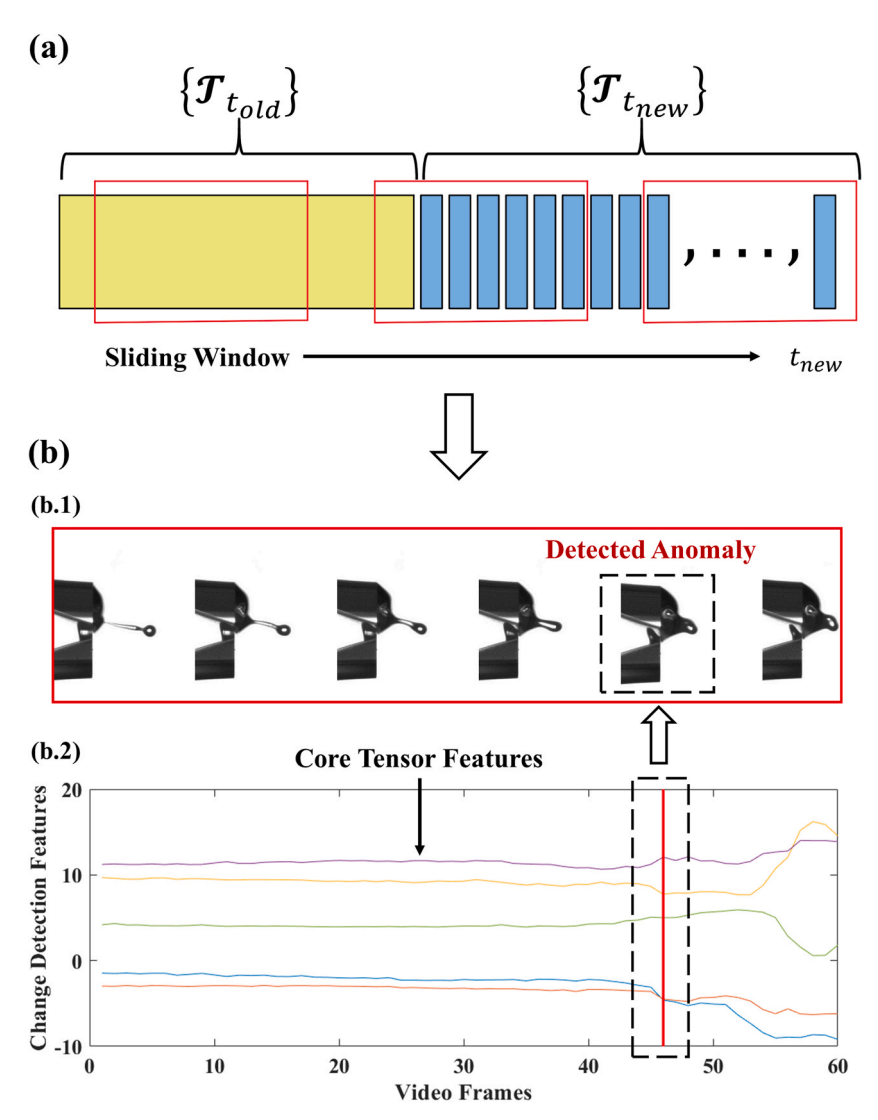


Fig. 5. An Illustration of the BOCD: (a) Sliding window scheme over the streaming data (i.e., LJP videos), and (b) Detection results (e.g., sliding window that contains the detected anomaly at frame 2449): (b.1) Frames before and after the detected anomaly, and (b.2) Temporal factorization matrix at the detected anomaly.

the length of the segment, and the temporal factorization matrix in the sliding window [12], BOCD computes the posterior probabilities of the current run length  $r_t$  that represents the probability of finding an anomaly in the recorded droplet video [12] via (see line 12 of Algorithm 1),

$$p(r_{t}|\boldsymbol{a}_{1:t}, r_{t-1}) = \frac{p(r_{t-1}|\boldsymbol{a}_{1:(t-1)}, r_{t-2})p(\boldsymbol{a}_{t}|\boldsymbol{a}_{1:(t-1)}, \boldsymbol{\eta})p(r_{t}|r_{t-1})}{p(\boldsymbol{a}_{1:t})}$$
(5)

where  $p(r_{t-1}|a_{1:(t-1)},r_{t-2})$  is the posterior probability at the previous time,  $p(a_t|a_{1:(t-1)},\eta)$  is the posterior distribution of the temporal factorization matrix at time t,  $p(r_t|r_{t-1})$  is the prior on the segment length, and  $p(a_{1:t})$  is the distribution of the detection features (i.e., vectorized temporal factorization matrix over sw). In the following, we will introduce each term in Eq. (5).

The posterior distribution for a new observation  $a_t$  is calculated as  $p(a_t|a_{1:(t-1)},\eta) = \int p(a_t|\theta,\eta)p(\theta|a_{1:(t-1)},\eta)d\theta$ , where  $\theta$  is a vector of segment parameters, with its hyperparameters  $\eta$ . Here,  $p(a_t|\theta,\eta)$  is the conjugate prior to  $p(a_t|a_{1:(t-1)},\eta)$ , thus the posterior probability for the incoming data can be found analytically and has the same form of the prior (see line 11 of Algorithm 1). Under the assumption that the incoming data follow a multivariate Gaussian distribution  $N(\mu,\Sigma)$ , BOCD detects the possible changes in  $\mu$  and  $\Sigma$ . In particular, the posterior

predictive probability,  $p(a_t|\mu^{(r_t)}, \Sigma^{(r_t)})$  will follow a normal inverse Wishart (NIW) distribution. In addition, following [12], the prior on the segment length is assumed to have a constant rate  $\phi$ , and is represented by  $p(r_t|r_{t-1}) = \frac{1}{\phi}$ .

As a result, the posterior in Eq. (5) can be computed to detect the droplet anomalies (see Fig. 5 (b)), represented by changes in  $\mu$  and  $\Sigma$ . The posterior is updated for each droplet video frame in the sliding window (see lines 9–20 of Algorithm 1), and Algorithm 1 returns the detected anomalies as the streaming data progress.

## 4. Case study

As mentioned in the Introduction, the timely droplet anomalies detection is crucial for the quality preservation of printed parts in the IJP process. For instance, droplet behaviors, such as the ones in Fig. 2 (b.2–b.4), may cause severe defects in the printed parts, hence affecting product functionality. In this section, we demonstrate the proposed framework for the timely and accurate droplet anomalies detection in the IJP process.

We used distilled water as ink/solution, and filled it into a syringe container (i.e., material reservoir in Fig. 2 (a)). The droplets were ejected and recorded as specified in Section 3.2, and we collected 4 videos using different settings (i.e., nozzle diameter, back-pressure, and

video length), as shown in Table 1. Here, video (1) and videos (2)–(4) were recorded with strobing delays of  $200\mu s$  and  $250\mu s$ , respectively, and at 30 fps.

We run Algorithm 1 on a desktop with an Intel(R) Xeon(R) W-2145 CPU @3.70 GHz and 64.0 GB of RAM. First, every incoming video frame  $\mathcal{T}_t \in \mathbb{R}^{480 \times 640}$ , which represents 1.5  $mm \times 2$  mm in the physical area and  $1pixel = 3.125 \ \mu m^2$ , is pre-processed as shown in Fig. 2 (d.1). During the pre-processing, we extract the sub-area corresponding to the shape of the droplet and further downsample (in terms of resolution) the image. As a result, we have  $\mathcal{T}_t \in \mathbb{R}^{30 \times 54}$  after the pre-processing.

We then perform the OnlineCP where the rank R and sliding window sw, are chosen as 5 and 60, respectively. After extensive simulation, it is determined that ranks R > 5 are sufficient to properly approximate the streaming tensor data in our case (see Figs. 6 (a) and 8 (a.3)). The sw size is determined to have a trade-off between anomaly detection accuracy and speed. Particularly, a too short sw may not guarantee the detection of anomaly since the BOCD method needs to gather evidence (some frames before and after an anomaly occurs) to determine whether an anomaly happens or not, while a too large sw will drastically affect the computational efficiency. Typically, sw > 50 is recommended to guarantee statistical significance and detect anomalies [44]. Therefore, we chose sw to cover 2 s (i.e., sw = 60) of the recorded IJP videos. After OnlineCP, we get the non-temporal factorization matrices,  $\mathbf{A}^{(1)} \in \mathbb{R}^{30 \times R}$ and  $A^{(2)} \in \mathbb{R}^{54 \times R}$ , and these are used to update the detection features  $a^{(3)} \in \mathbb{R}^{sw \times R}$  in the specified sliding window (see Fig. 5 (b)). Concisely, sw corresponds to the number of frames that entails the sliding window. Finally, the detection features allocated in the vectorized temporal factorization matrices  $a^{(3)}$  serve as the inputs for BOCD. The droplet anomalies are detected accurately, see representative examples in Fig. 6 (b). In the following, we use video (1) to demonstrate the anomaly detection results and computational performance. Fig. 6 (a) shows the tensor reconstruction results for frames 550 and 564, the first pair of actual and detected anomalies. From Fig. 6 (a), the OnlineCP can accurately approximate the streaming video. As shown in Fig. 6 (b), the anomaly starts some frames before it is detected, and this is because BOCD needs to accumulate some frames to corroborate that a change really happens. In addition, the performance of BOCD is affected by the distribution properties of the features extracted from OnlineCP, hence the closer to a normal distribution the features are, the better the BOCD performs. For instance, Fig. 7 (a-b) show QQ plots corresponding to features extracted from two different segments. The latter derives into relatively big detection delays, where the anomaly is detected at frame 632, while the corresponding actual anomaly happens at frame 615. The time consumption of Algorithm 1 per frame (i.e., from line 2 to line 20, including OnlineCP, detection feature extraction, and BOCD) is reported in Fig. 7 (c), where the worst-case scenario takes 0.0300 s and the best-case scenario takes 0.0161 s (the average time is 0.0246 s). Based on the average time to process a frame in the streaming video, the proposed framework is able to analyze up to 40 fps, which is fast enough for online anomaly detection in our case.

Additional analysis is performed to study the effects of varying *R* and *sw* on the proposed framework, as shown in Fig. 8. Fig. 8 (a.1) and (b.1) show how the accuracy of the proposed framework is impacted by the *R* and *sw* selection. Large values of *R* and *sw* will not necessarily increase the detection accuracy of the method. For instance, high rank values may not guarantee the normality assumption of the extracted features and this impacts the detection accuracy of the BOCD (see Fig. 8 (a.1)). On the other hand, large *sw* sizes may include multiple change points within each sliding window [44], hence disturbing the detection accuracy (see Fig. 8 (b.1)). Furthermore, as expected, large values of *R* and *sw* will increase the computational time per frame processed, as shown in Fig. 8 (a.2) and (b.2), respectively. Fig. 8 (a.3) shows that higher ranks benefit the LJP streaming video frames reconstruction. The *R* and *sw* selection is a case-specific process and depends on system setup, camera, etc.

The proposed framework was also evaluated under different settings. namely nozzle size and back-pressure, as shown in the videos (2)-(4) of Table 1. The detection results and comparison are shown in Fig. 9, where Fig. 9 (a) shows a normal droplet evolution at different strobing delays, Fig. 9 (b.1-b.2) display a comparison of the detection results for different settings (videos (2)-(3) in Table 1), and Fig. 9 (b.3) presents a normal process where no anomalies happen in the IJP process (video (4) in Table 1). If the droplet is adequately formed at initial stages (e.g., 100  $\mu$ s), it is very likely to have a droplet of good quality for the printing process, see strobing delay  $1000 \,\mu s$  in Fig. 9 (a). Consequently, the comparison was performed at a strobing delay of 250 µs. Fig. 9 (b.1) shows the actual and detected frames of anomalies for IJP with a nozzle diameter of 50  $\mu m$ . After varying the back-pressure, at frame 720 the droplet suffers from a displacement to the right of the nozzle and subsequently a satellite surrounds the droplet at frame 762, and these anomalies were timely detected by the proposed method. Furthermore, Fig. 9 (b.2) shows actual and detected frames for severe anomalies induced by the settings displayed in video (3) of Table 1. Here, the initial droplet is shown to be normal, and once the back-pressure is severely increased, a blockage is generated as shown in frame 149 (absence of droplet). Afterwards, the pressure was drastically increased causing an overflow, as can be seen in frame 820. These anomalies were accurately detected. Finally, Fig. 9 (b.3) shows a droplet that does not suffer from any anomaly during the process, and the proposed framework did not detect any change as the streaming, i.e., IJP video, progressed.

The capabilities of the proposed framework were hitherto demonstrated by Figs. 6–9. Complementary to this, we numerically evaluate the detection performance with anomaly detection precision, recall, and F-1 measures for time series [45]. Traditionally, these metrics have been concerned with evaluating point-based anomalies, while our case requires range-based evaluation since the LJP anomalies occur over the

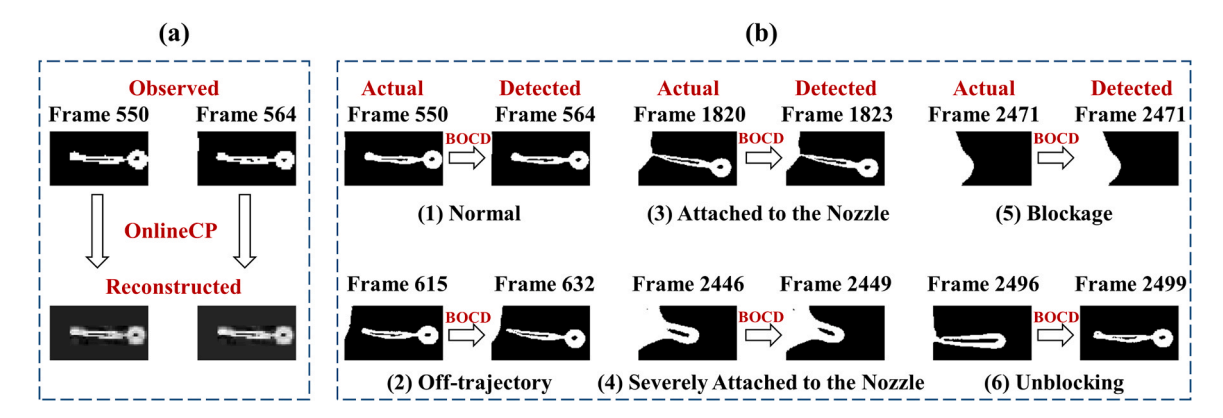


Fig. 6. Proposed framework detection results: (a) Observed and reconstructed tensors (i.e., video frames) and (b) Representative actual versus detected droplet anomalies frames in various scenarios.

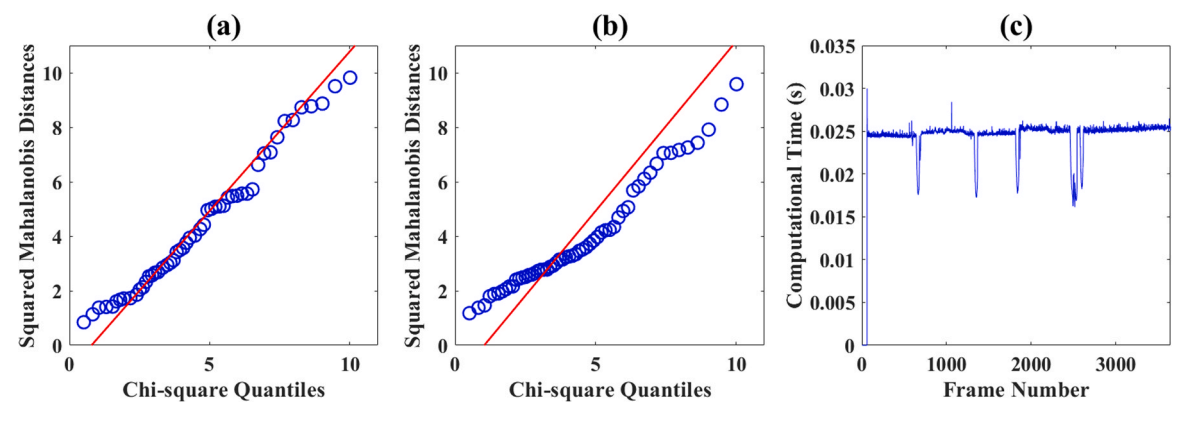


Fig. 7. Proposed framework computational performance: (a) QQ plot for features (sw segment containing frame 564), (b) QQ plot for features (sw segment containing frame 632), and (c) Computational time per frame processed.

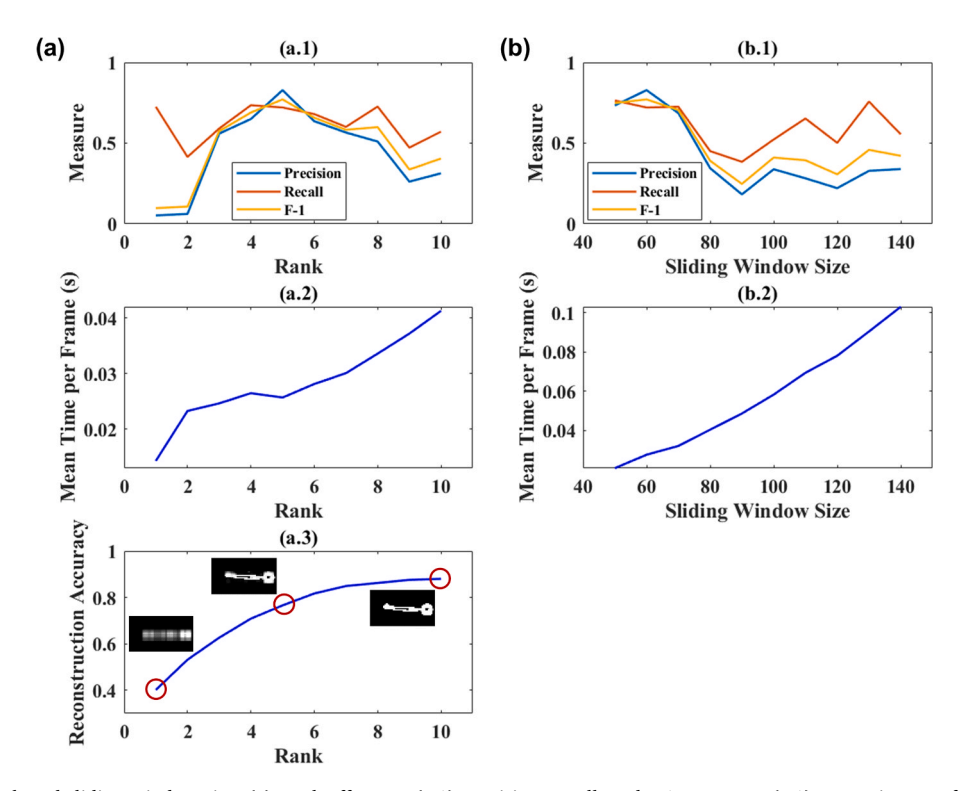


Fig. 8. The impact of rank and sliding window size: (a) Rank effect on: (a.1) Precision, recall, and F-1 measures, (a.1) Mean time per frame processed, and (a.3) Tensor reconstruction, (b) Sliding window size effect on: (b.1) Precision, recall, and F-1 measures and (b.2) Mean time per frame processed.

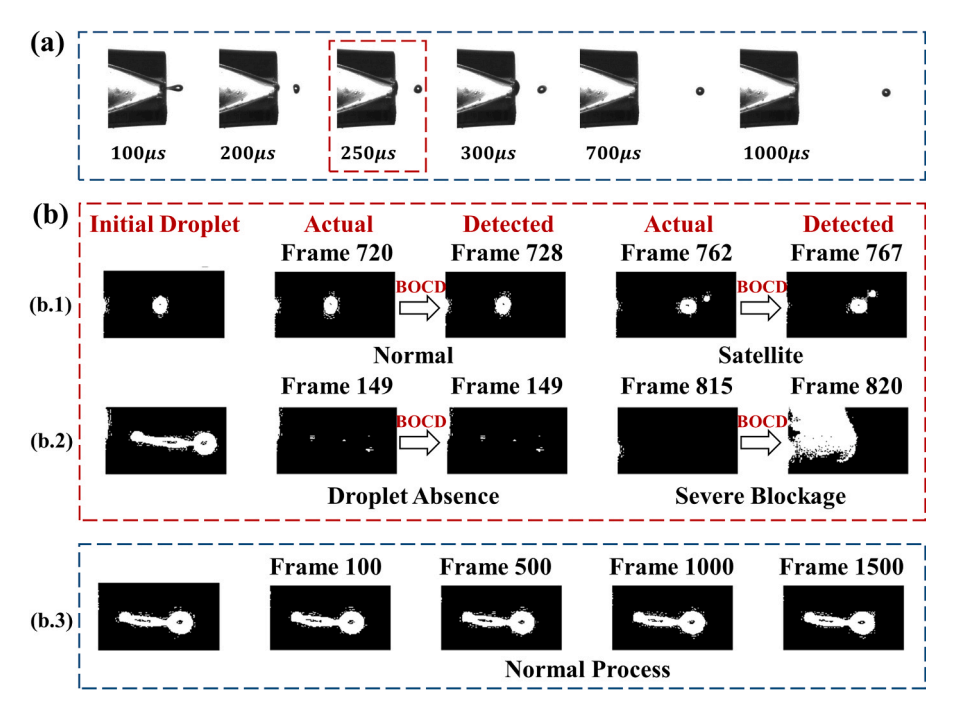
course of time. Based on the classical definitions of  $Precision = \frac{TP}{TP+FP}$  and  $Recall = \frac{TP}{TP+FP}$ , where TP is true positive, FP is false positive, and FN is false negative, Tatbul et al. [45] extended these concepts to range-based evaluations. Specifically, these metrics are performed on the overlap between the actual and detected ranges [45]. For example, the actual range of frames [550,615] and the detected range of frames [564,632] in Fig. 6(b).

Fig. 10 shows an overall evaluation for the performance of the proposed framework. Generally, the larger the overlap between actual and detected ranges, the higher the measures are going to be. From Fig. 10, the proposed framework can timely and accurately detect the anomalies in the IJP process. Although our method showed to be very accurate when drastic anomalies happen (Fig. 9 (b.2)), a detection delay occurs when the anomalies progressively appear (Fig. 6 (b)), and this is reflected on the measures of video (1) in Fig. 10. Nevertheless, the delay for the worst case scenario in video (1) is 17 frames, which is approximately 0.57 s delay, and this will not hamper the anomalies detection.

In summary, the proposed online droplet anomaly detection framework can accurately and efficiently detect the anomalies in IJP and can pave the way for achieving real-time control. The proposed framework can be applied to a broad range of ink/solution materials, since it only depends on the droplet videos (i.e., shape of the droplets regardless of the material), and other fast changing processes.

## 5. Conclusion and discussion

IJP is capable of producing parts with high-quality and high-resolution using a wide variety of materials. However, the droplet behavior is vulnerable to a lot of dynamic process and ambient conditions, and the quality of the printed parts can be harmed by the abrupt droplet anomalies. Detecting these abrupt anomalies is important but has been very challenging in the literature. In this work, we propose an online framework that is capable to timely detect anomalies from real-time videos. The novelties of this paper include the online change



**Fig. 9.** Detection comparison results for different disturbance regimes: (a) Droplet evolution of a normal IJP jetting behavior, (b) Representative detection results: (b.1) Nozzle diameter 50  $\mu m$ , (b.2) Nozzle diameter 100  $\mu m$ , and (c) Normal process with nozzle diameter 100  $\mu m$ .

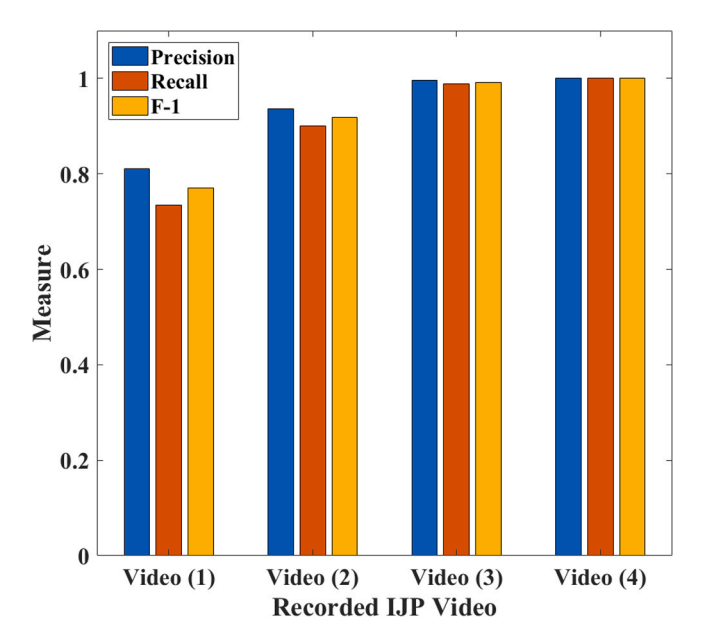


Fig. 10. Anomaly detection precision, recall, and F-1 measures for each video.

detection of the streaming data, and no baseline data is required for feature extraction and subsequent anomalies identification. The proposed framework detection and computational performance show promising results towards achieving real-time change detection and control in IJP processes. The framework can be applied to problems with streaming data recorded from other AM processes and beyond with complex process dynamics.

There are several potential research directions that can be pursued in the future. One direction is to further accelerate the OTF by incorporating compressed sketch multiplications into the OnlineCP method. Another direction is to extend this framework so that it can handle non-parametric streaming data. Finally, hardware capabilities may cause detection delays, which may affect the framework performance.

Incorporating advanced hardware modules might reduce not only the computational time of running the algorithm but also the operational time cost, which will be investigated in the future.

#### CRediT authorship contribution statement

Luis Javier Segura: Conceptualization, Methodology, Software, Formal analysis, Writing - original draft, Writing - review & editing. Tianjiao Wang: Investigation, Writing - review & editing. Chi Zhou: Conceptualization, Writing - review & editing. Hongyue Sun: Conceptualization, Methodology, Writing - review & editing.

## **Declaration of Competing Interest**

The authors declare that they have no known competing financial interests or personal relationships that could have appeared to influence the work reported in this paper.

## Acknowledgement

This work is partially supported by the NSF Grant No. CMMI-1846863 and Sustainable Manufacturing and Advanced Robotics Technologies, Community of Excellence (SMART CoE) at the State University of New York at Buffalo.

## References

- J.D. Prince, 3d printing: an industrial revolution, J. Electron. Resour. Med. Libr. 11 (1) (2014) 39–45.
- [2] J. Huang, L.J. Segura, T. Wang, G. Zhao, H. Sun, C. Zhou, Unsupervised learning for the droplet evolution prediction and process dynamics understanding in inkjet printing. Addit. Manuf. (2020), 101197.
- [3] M. Singh, H.M. Haverinen, P. Dhagat, G.E. Jabbour, Inkjet printing process and its applications, Adv. Mater. 22 (6) (2010) 673–685.
- [4] S.D. Hoath, Fundamentals of Inkjet Printing: The Science of Inkjet and Droplets, John Wiley & Sons., 2016.
- [5] O.A. Basaran, H. Gao, P.P. Bhat, Nonstandard inkjets, Annu. Rev. Fluid Mech. 45 (2013) 85–113.
- [6] M.H. Tsai, W.S. Hwang, H. Chou, The micro-droplet behavior of a molten lead-free solder in an inkjet printing process, J. Micromech. Microeng. 19 (12) (2009), 125021.

- [7] J. Kechagias, P. Stavropoulos, A. Koutsomichalis, I. Ntintakis, N. Vaxevanidis, Dimensional accuracy optimization of prototypes produced by polyjet direct 3D printing technology, Adv. Eng. Mech. Mater. (2014) 61–65.
- [8] B.T. Lies, Y. Cai, E. Spahr, K. Lin, H. Qin, Machine vision assisted micro-filament detection for real-time monitoring of electrohydrodynamic inkjet printing, Procedia Manuf. 26 (2018) 29–39.
- [9] T. Wang, C. Zhou, W. Xu, Online droplet monitoring in inkjet 3d printing using catadioptric stereo system, IISE Trans. 51 (2) (2019) 153–167.
- [10] H. Yan, K. Paynabar, J. Shi, Image-based process monitoring using low-rank tensor decomposition, IEEE Trans. Autom. Sci. Eng. 12 (1) (2014) 216–227.
- [11] D.C. Montgomery, Introduction to Statistical Quality Control, John Wiley & Sons,, 2007.
- [12] I. Lauzana, Online change-point detection algorithm for multi-variate data: Applications on human/robot demonstrations, (2018). https://github.com/epfl-lasa/changepoint-detection.
- [13] S. Zhou, N.X. Vinh, J. Bailey, Y. Jia, I. Davidson, Accelerating online cp decompositions for higher order tensors, in: Proceedings of the 22nd ACM SIGKDD International Conference on Knowledge Discovery and Data Mining, (2016), 1375–1384
- [14] L.J. Segura, C. Narvaez-Munoz, C. Zhou, H. Sun, Sketch-based tensor decomposition for non-parametric monitoring of electrospinning processes, in: Proceedings of the International Manufacturing Science and Engineering Conference, American Society of Mechanical Engineers, (2020), (Accepted).
- [15] J. Abu-Khalaf, L. Al-Ghussain, A. Nadi, R. Saraireh, A. Rabayah, S. Altarazi, A. Al-Halhouli, et al., Optimization of geometry parameters of inkjet-printed silver nanoparticle traces on pdms substrates using response surface methodology, Materials 12 (20) (2019) 3329.
- [16] Z. Zhou, L.R. Cantu, X. Chen, M.R. Alexander, C.J. Roberts, R. Hague, C. Tuck, D. Irvine, R. Wildman, High-throughput characterization of fluid properties to predict droplet ejection for three-dimensional inkjet printing formulations, Addit. Manuf. 29 (2019), 100792.
- [17] H. Wijshoff, Drop dynamics in the inkjet printing process, Curr. Opin. Colloid Interface Sci. 36 (2018) 20–27.
- [18] X. Wang, M. Yuan, X. Xiong, M. Chen, M. Qin, L. Qiu, H. Lu, G. Zhang, G. Lv, A. H. Choi, Process optimization for inkjet printing of triisopropylsilylethynyl pentacene with single-solvent solutions, Thin Solid Films 578 (2015) 11–19.
- [19] A. Lee, K. Sudau, K.H. Ahn, S.J. Lee, N. Willenbacher, Optimization of experimental parameters to suppress nozzle clogging in inkjet printing, Ind. Eng. Chem. Res. 51 (40) (2012) 13195–13204.
- [20] L. Zhou, L. Yang, M. Yu, Y. Jiang, C.-F. Liu, W.-Y. Lai, W. Huang, Inkjet-printed small-molecule organic light-emitting diodes: halogen-free inks, printing optimization, and large-area patterning, ACS Appl. Mater. Interfaces 9 (46) (2017) 40533–40540.
- [21] Z. Xiong, C. Liu, Optimization of inkjet printed PEDOT:PSS thin films through annealing processes, Org. Electron. 13 (9) (2012) 1532–1540.
- [22] S. Rahul, K. Balasubramanian, S. Venkatesh, Optimizing inkjet printing process to fabricate thick ceramic coatings, Ceram. Int. 43 (5) (2017) 4513–4519.
- [23] J. Mueller, K. Shea, C. Daraio, Mechanical properties of parts fabricated with inkjet 3d printing through efficient experimental design, Mater. Des. 86 (2015) 902–912.
- [24] G. Cummins, R. Kay, J. Terry, M.P. Desmulliez, A.J. Walton, Optimization and characterization of drop-on-demand inkjet printing process for platinum organometallic inks, in: Proceedings of the 2011 IEEE 13th Electronics Packaging Technology Conference, IEEE, (2011), 256–261.

- [25] R. Das, A.K. Ball, S.S. Roy, Parametric optimization of e-jet based micro manufacturing system through hybrid taguchi methodology, Mater. Today Proc. 5 (2) (2018) 6981–6989.
- [26] N.F. Morrison, O.G. Harlen, Viscoelasticity in inkjet printing, Rheol. Acta 49 (6) (2010) 619–632.
- [27] A. van der Bos, M.-J. van der Meulen, T. Driessen, M. van den Berg, H. Reinten, H. Wijshoff, M. Versluis, D. Lohse, Velocity profile inside piezoacoustic inkjet droplets in flight: comparison between experiment and numerical simulation, Phys. Rev. Appl. 1 (1) (2014), 014004.
- [28] D. Bartolo, A. Boudaoud, G. Narcy, D. Bonn, Dynamics of non-newtonian droplets, Phys. Rev. Lett. 99 (17) (2007), 174502.
- [29] K. Rahman, J.-B. Ko, S. Khan, D.-S. Kim, K.-H. Choi, Simulation of droplet generation through electrostatic forces, J. Mech. Sci. Technol. 24 (1) (2010) 307–310.
- [30] M. Khanzadeh, W. Tian, A. Yadollahi, H.R. Doude, M.A. Tschopp, L. Bian, Dual process monitoring of metal-based additive manufacturing using tensor decomposition of thermal image streams, Addit. Manuf. 23 (2018) 443–456.
- [31] F.M. Megahed, L.J. Wells, J.A. Camelio, W.H. Woodall, A spatiotemporal method for the monitoring of image data, Qual. Reliab. Eng. Int. 28 (8) (2012) 967–980.
- [32] H. Sun, K. Wang, Y. Li, C. Zhang, R. Jin, Quality modeling of printed electronics in aerosol jet printing based on microscopic images, J. Manuf. Sci. Eng. 139 (7) (2017).
- [33] H. Yan, M. Grasso, K. Paynabar, B.M. Colosimo, Real-time detection of clustered events in video-imaging data with applications to additive manufacturing, arXiv preprint arXiv:2004.10977.
- [34] C. Hawkins, Z. Zhang, Variational bayesian inference for robust streaming tensor factorization and completion, in: Proceedings of the 2018 IEEE International Conference on Data Mining (ICDM), IEEE, (2018), 1446–1451.
- [35] M. Mardani, G. Mateos, G.B. Giannakis, Subspace learning and imputation for streaming big data matrices and tensors, IEEE Trans. Signal Process. 63 (10) (2015) 2663–2677.
- [36] H. Kasai, Online low-rank tensor subspace tracking from incomplete data by cp decomposition using recursive least squares, in: Proceedings of the 2016 IEEE International Conference on Acoustics, Speech and Signal Processing (ICASSP), IEEE, (2016), 2519–2523.
- [37] S. Aminikhanghahi, D.J. Cook, A survey of methods for time series change point detection, Knowl. Inf. Syst. 51 (2) (2017) 339–367.
- [38] Y. Li, G. Lin, T. Lau, R. Zeng, A review of changepoint detection models, arXiv preprint arXiv:1908.07136.
- [39] R.P. Adams, D.J. MacKay, Bayesian online changepoint detection, arXiv preprint arXiv:0710.3742.
- [40] Y. Kawahara, M. Sugiyama, Change-point detection in time-series data by direct density-ratio estimation, in: Proceedings of the 2009 SIAM International Conference on Data Mining, SIAM, (2009), 389–400.
- [41] F. Desobry, M. Davy, C. Doncarli, An online kernel change detection algorithm, IEEE Trans. Signal Process. 53 (8) (2005) 2961–2974.
- [42] S. Li, Y. Xie, H. Dai, L. Song, Scan b-statistic for kernel change-point detection, Seq. Anal. 38 (4) (2019) 503–544.
- [43] J. Sun, D. Tao, C. Faloutsos, Beyond streams and graphs: dynamic tensor analysis, in: Proceedings of the 12th ACM SIGKDD international conference on Knowledge discovery and data mining, (2006), 374–383.
- [44] Z. Harchaoui, E. Moulines, F.R. Bach, Kernel change-point analysis, Adv. Neural Inf. Process. Syst. (2009) 609–616.
- [45] N. Tatbul, T.J. Lee, S. Zdonik, M. Alam, J. Gottschlich, Precision and recall for time series, Adv. Neural Inf. Process. Syst. (2018) 1920–1930.